Effects of cobalt doping and three-dimensionality in $BaFe_2As_2$

A. F. Kemper,* C. Cao, P. J. Hirschfeld, and H.-P. Cheng
Department of Physics, University of Florida, Gainesville, Florida 32611, USA
(Received 8 April 2009; published 25 September 2009)

We investigate the dual roles of a cobalt impurity in the Ba-122 ferropnictide superconductor in the state with coexisting collinear spin-density wave (SDW) order as a dopant and as a scattering center, using first-principles electronic-structure methods. The Co atom is found to dope the FeAs plane where it is located with a single delocalized electron as expected, but also induces a strong perturbation of the SDW ground state of the system. This in turn induces a stripelike modulation of the density of states in nearby planes which may be observable in scanning tunnel microscope (STM) experiments. The defect is found to have an intermediate strength nonmagnetic scattering potential with a range of roughly 1 Å, and the Co gives rise to a smaller but longer range magnetic scattering potential. The impurity potential in both channels is highly anisotropic, reflecting the broken symmetry of the SDW ground state. We give values for the effective Co potentials for each *d* orbital on the impurity and nearby sites. The calculation also shows a clear local resonance comprised of Co states about 200 meV above the Fermi level, in quantitative agreement with a recent report from STM. Finally, we discuss the issue of the effective dimensionality of the 122 materials, and show that the hybridization of the out-of-phase As atoms leads to a higher density of states between the FeAs planes relative to the 1111 counterparts.

DOI: 10.1103/PhysRevB.80.104511 PACS number(s): 74.25.Jb, 71.20.−b, 74.62.Dh

I. INTRODUCTION

The recent discovery of superconductivity in the oxypnictide systems *R*OFeAs, where *R* is one of the rare earths La, Sm, Pr, Nd, and Gd, has generated a great deal of interest in these and related compounds. Soon thereafter, superconductivity was reported upon hole doping of the oxygen-free pnictides RFe_2As_2,[1,2] where *R* in this case is one of the alkaline earth metals Ca, Sr, and Ba, formed in the $ThCr_2Sr_2$ structure. In the *R*OFeAs-type materials (which we refer to as "1111") critical temperatures of 56 K have been achieved,[3] whereas in the RFe_2As_2-type materials ("122"), T_c has thus far been limited to 38 K.[1] In the latter materials, the initial (hole) doping was accomplished by substitution of the alkaline earth metal by an alkali, such as K.[1]

With the discovery of superconductivity at 22K upon cobalt doping of $BaFe_2As_2$ by Sefat *et al.*,[4] the oxygen-free 122 pnictide materials have now been shown to also superconduct upon electron doping. Since single crystals of relatively high quality can be grown without the difficulty of handling the alkali dopant, these materials have become quite popular for investigation of fundamental properties of the Fe pnictides. Furthermore, the Co atom substitutes directly for an Fe, in the FeAs plane where it is believed that pairing and magnetism originate. After doping the plane, the nominal electronic configuration of Co is quite similar to the Fe it replaces, but represents an effective scattering potential localized primarily in the plane as well. One might expect that the scattering potential sampled by quasiparticles in the FeAs plane due to a Co would be considerably larger than an out-of-plane alkali dopant due to its location in the plane; however this argument, familiar from the cuprates, must be critically examined if the systems are more three-dimensional in nature.

Another possibly important difference between Co and the alkali dopant is related to spin: cobalt frequently has a strong intrinsic magnetic moment, and in its metallic form it orders ferromagnetically. The Fe-pnictide superconductors manifest a "spin-density wave" (SDW) ordering transition at high temperatures, and enhanced spin fluctuations due to proximity to the SDW state have been suggested as a pairing mechanism.[5–13] Thus, one can expect that the introduction of an ion with a different magnetic moment than Fe will have a strong effect on the SDW state. Indeed, it is found that Co doping suppresses and splits the magnetic and structural phase transitions, which are degenerate in the 122 parent compounds.[14] The magnetic transition temperature, which is suppressed more rapidly, continues to decrease as superconductivity arises; therefore a range of Co doping corresponds to a coexistence of the two states,[15–20] which recent NMR experiments have shown to be homogeneous at the atomic scale.[21] To understand the destruction of the SDW by doping, as well as the possibilities of coexistence of the two states, it will be interesting to investigate the effect of the Co dopant on the SDW locally, and to ask to what extent Co acts as a magnetic or nonmagnetic scatterer.

The Fe pnictides are of great importance not only because of their potentially high critical temperatures, but also because they provide the possibility of comparing the even higher temperature cuprate materials to another class of high-T_c superconductors. It is frequently speculated that superconductivity at high temperatures arises in the cuprates because of their highly layered nature which enhances electronic correlations. With the discovery of the 1111 ferropnictides, DFT calculations indicated that the density of states near the Fermi level was localized in the FeAs planes, and that the Fermi surfaces were nearly two-dimensional, weakly corrugated cylinders.[22] The 122s are similar in this respect, as reported by LDA studies,[4] but have a distinctly larger z dispersion in some of the bands; and Fermi surfaces near the M points appear to have significantly larger corrugations. In addition, several studies have recently reported an unexpectedly small anisotropy in *c*-axis versus *a*-axis resistivity, pen-

etration depth, and upper critical field.[19,23] To investigate further, Prozorov *et al.*[24] compared the anisotropy in the London penetration depth for $Ba_{1-x}K_xFe_2As_2$, $Ba(Fe_{1-x}Co_x)_2As_2$, and $NdFeAs(O_{1-x}F_x)$, and reported low-temperature ratios (λ_c/λ_a) of approximately 6, 7, and 18, respectively. These data suggest that the iron-based 122 superconductors are quite complex compared to the cuprates, with multisheeted Fermi surfaces, at least some of which are quite three-dimensional. It is not yet clear why these materials are more three-dimensional, if the three-dimensional character is a strong function of doping, or if this property is useful or harmful for superconductivity.

In this paper, we shall address the effect of Co doping in $BaFe_2As_2$ using first-principles calculations. We find that, in the SDW state, Co dopes the system with a single electron as expected, and that it breaks the symmetry between spin-up and -down electrons. The resulting scattering potential is found to be of order the effective bandwidth in the system, making it an intermediate-strength potential scatterer, while the magnetic part of the potential is considerably smaller, but quite long range. The potential in both channels displays a strongly anisotropic twofold character reflecting the collinear SDW. Curiously, although we find that the Co electron principally dopes the FeAs plane where it is located, there are also significant effects on the local density of states of neighboring planes, which may be visible to scanning tunnel microscope (STM). Localized Co resonances at −800 and +200 meV should also be observable in STM. Finally, we discuss the origin of the reported anisotropy of the 122s, as compared to the 1111s. We find that the interplane local density of states near the Fermi surface has a strong As p_z character. Due to the different symmetry positions that the As atoms occupy in the 1111s as compared to the 122s, there is a stronger overlap of the As p_z orbitals in the 122s, which gives the 122s their comparatively stronger three-dimensional nature. Co doping appears to suppress this hybridization.

II. CALCULATIONAL DETAILS AND STRUCTURE

The structural-relaxation calculations were performed using density-functional theory (DFT) (Refs. 25 and 26) within the generalized gradient approximations as implemented in the QUANTUM-ESPRESSO (Ref. 27) package, which uses a plane wave basis. We used the Perdew-Burke-Ernzerhof[28] exchange-correlation functionals and ultrasoft pseudopotentials. The use of ultrasoft pseudopotentials enabled us to utilize an energy cutoff of 40 Ry for the plane wave basis, while the density cutoff was taken to be 400 Ry. For the calculations in the paramagnetic state, we considered Ba122 in the tetragonal I4/mmm structure (see Fig. 1), where we used lattice constants $a=3.9625$ Å and $c=13.0168$ Å as obtained by Rotter *et al.*[29] for the structure at 297 K. For the undoped SDW state, which is in the orthorhombic Fmmm state, we used $a=5.6146$ Å, $b=5.5742$ Å, and $c=12.9453$ Å. To consider a doping $x=1/16$, we used a supercell of 40 atoms (16 Fe atoms) and replaced a single Fe by Co. In the actual material, however, the dopant is not placed preferentially in one plane over another; all planes are equally likely to be

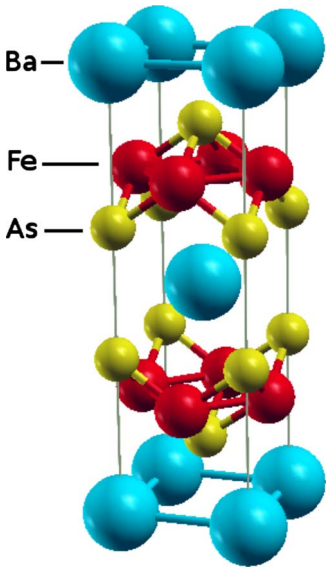

FIG. 1. (Color online) Structure of $BaFe_2As_2$.

doped. To address this issue, we have additionally done calculations for an even larger cell of 80 atoms (32 Fe atoms) where two Fe atoms were replaced. The lattice constants for the doped calculation were kept the same as for the undoped SDW state. In all the cases reported except the 80-atom cells, the atomic positions were optimized. Where appropriate, we have checked using the 40-atom cell that the quantity reported for the 80-atom cell does not vary appreciably upon relaxation.

III. COMPARISON OF THE SPIN-DENSITY WAVE AND PARAMAGNETIC STATE

The $BaFe_2As_2$ system has been experimentally observed to support a SDW state, where the spins are aligned along lines in the (110) direction in the plane, and the planes are coupled antiferromagnetically.[30,31] Figure 2 shows the

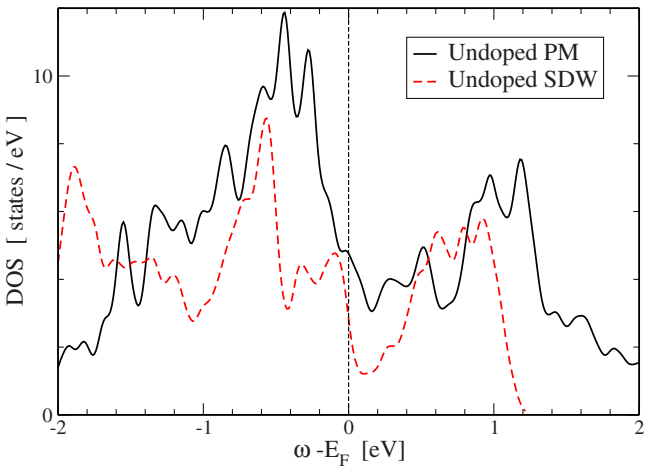

FIG. 2. (Color online) DOS for $BaFe_2As_2$ in the undoped PM and undoped SDW states. The Fermi levels for both systems have been aligned at 0.

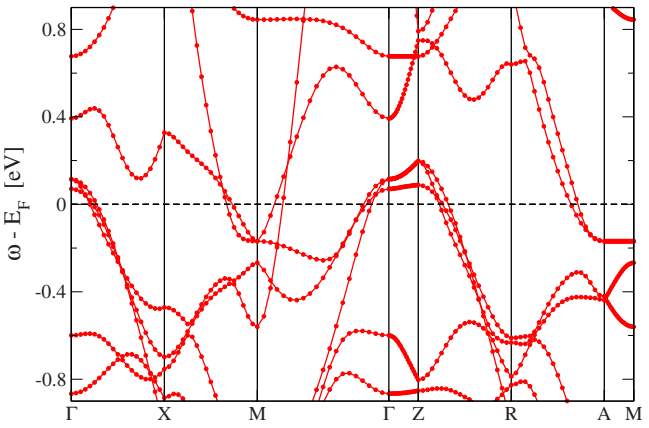

FIG. 3. (Color online) Undoped PM band structure along high-symmetry lines.

density of states for undoped $BaFe_2As_2$ in the SDW and paramagnetic (PM) states. There is a clear difference in peak structure, as well as a drop in the density of states (DOS) at the Fermi level from the PM to the undoped SDW state. As discussed by Zhang *et al.*,[32] the drop in the DOS may be caused by the removal of the incipient magnetic instability associated with the peak in the PM DOS and the possibility of Fermi surface nesting.

To further study the difference in electronic structure, we have calculated the band structure for both states, which are shown in Figs. 3 and 4. For easier comparison, we have used the tetragonal cell and its high-symmetry points in all band structure plots. As can be seen from the figures, the band structure of the SDW state is entirely different from that of the PM state. The PM band structure, in agreement with that reported by other studies,[4,33–35] has hole pockets around the Γ point and electron pockets around M. Since these pockets are of similar size, there is a large potential for nesting. In the SDW state, on the other hand the nesting has entirely disappeared. Furthermore, there are Fermi surface crossings from R to A in the PM state which are not found in the SDW state.

IV. EFFECT OF CO DOPING

To investigate the effect of cobalt doping, we used several sets of atomic configurations, with one of every 16 iron atoms replaced by a Co atom, yielding a concentration of 6.25% and an empirical formula of $Ba(Fe_{0.9375}Co_{0.0625})_2As_2$, which is well within the experimentally determined range for the SDW state as reported by several studies.[15–20] The configurations considered are shown in Fig. 5. We shall refer to the configuration with a single Co dopant as configuration A, and to those with two Co dopants as configuration B for unlike-spin dopants, and configuration C for like-spin dopants. For configuration A, the ions were allowed to relax (all within the SDW state) after Co substitution. The majority of displacements occurred near the dopant site, where the Co atom pushes away the Fe atoms that lie along the line of collinear spins in the SDW state. Furthermore, the Co atom attracts the nearest As atoms, causing the distance to decrease by 0.03 Å compared to the normal Fe-As distance.

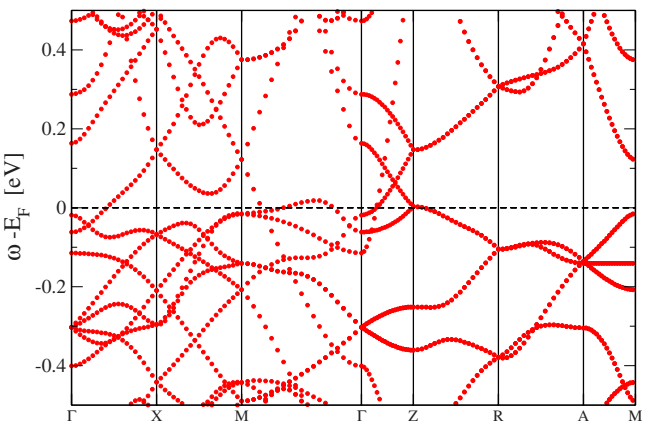

FIG. 4. (Color online) Undoped SDW band structure along high-symmetry lines. Due to symmetry in up and down spins, the individual spin states are degenerate and thus only one is shown.

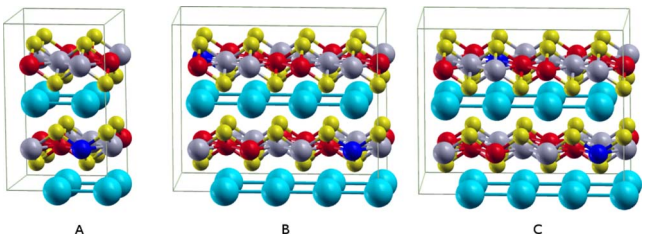

FIG. 5. (Color online) Configurations of $Ba(Fe_{1-x}Co_x)_2As_2$ for $x=\frac{1}{16}$, in the SDW state. (a) 40-atom unit cell with a single Co dopant, (b) 80-atom unit cell with two Co dopants of opposite spin, and (c) 80-atom unit cell with two Co dopants of same spin. Ba atoms are light blue, As atoms are yellow, gray and red balls denote Fe atoms of up and down spin, and the Co dopants are dark blue. Note that configurations B and C have 2 Co dopants each, while maintaining the same concentration.

Initially limiting considerations to configuration A, we observe that Co doping induces a small shift in the overall density of states near the Fermi level (see Fig. 6). When the Fermi levels are aligned, the doped and undoped DOSs are similar in shape, suggesting that a rigid band approach to doping the system is qualitatively valid. However, a closer look will reveal that there are other effects not captured by a rigid band shift.

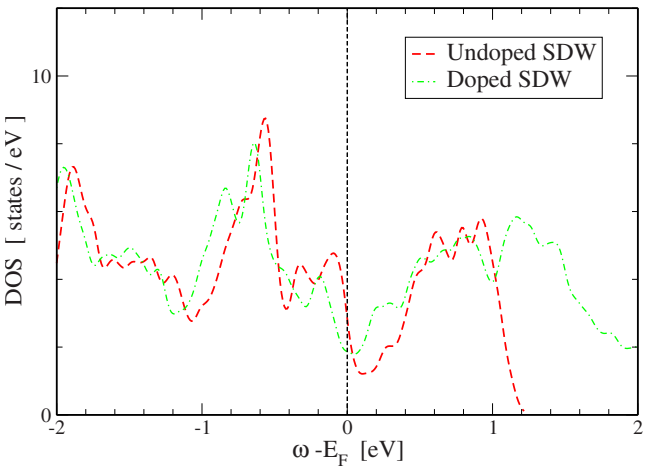

FIG. 6. (Color online) DOS for $Ba(Fe_{1-x}Co_x)_2As_2$ in the undoped and doped configuration A, SDW states. The Fermi levels for both systems have been aligned at 0.

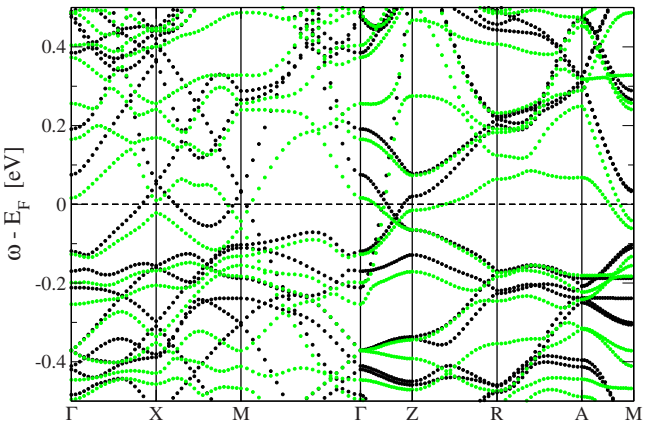

FIG. 7. (Color online) Doped SDW band structure along high-symmetry lines. Black (green) indicates the majority (minority) spin.

To investigate the effect of the Co dopant on the spin structure of the system, we have calculated the band structure along high-symmetry directions, as shown in Fig. 7. It is immediately obvious from the picture that the degeneracy between spin up and down electrons is broken. The presence of the Co dopant changes the net spin of the system from 0 to $0.46\mu_B$/cell. Cobalt not only renormalizes the moment on the site where it substitutes for Fe, however, but is found to have a strong nonlocal effect, decreasing the magnetization over the entire plane. Some of the polarization is spread from the Co site to the other Fe sites in the doped plane ($0.05-0.10\mu_B$ per Fe ion) (Fig. 8). Additionally, the presence of the Co ion enhances the polarization in the undoped layer (in configuration A), increasing the absolute spin per ion by approximately $0.05\mu_B$.

The electron doping also raises the overall Fermi energy, but since the spin degeneracy is broken, does so differently for the majority versus the minority spin. Furthermore, the

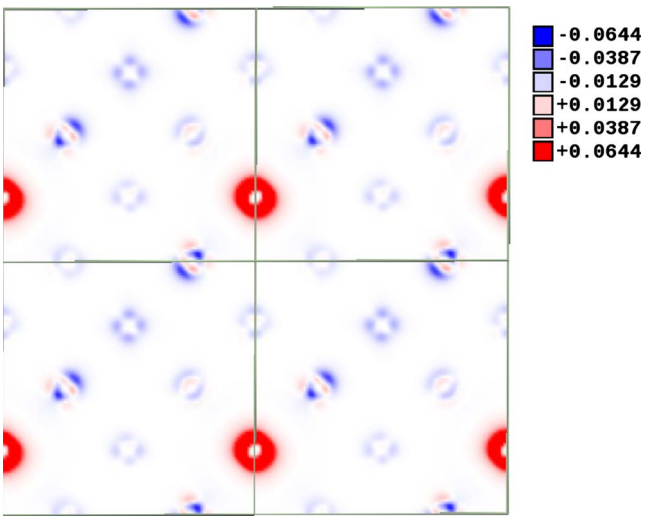

FIG. 8. (Color online) Local spin polarization in the dopant plane. A relatively large polarization is induced around the dopant site, in addition to a change in polarization on nearby Fe sites of like spin.

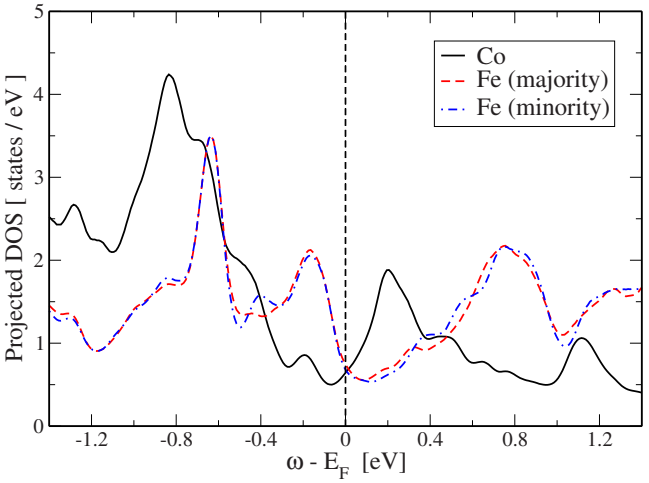

FIG. 9. (Color online) PDOS for atomic species Co (dashed) and Fe (solid). The Fe states belong to atoms in the unit cell located as far as possible from the Co.

number and character of the bands crossing the Fermi surfaces change greatly. After doping, two minority spin bands cross the Fermi level from A to M, and a number of crossings have appeared from X to M. It is interesting to ask which of the states remaining near the Fermi level have Co character, which might enable imaging of the Co atoms on the surface of this system by STM, as was done successfully with O dopants in the high-T_c superconductor $Bi_2Sr_2CaCu_2O_{8+x}$.[36] This can be accomplished by plotting the partial density of states (PDOS) projected onto atomic orbitals of a given species. In Fig. 9, we compare the density of Co states in the doped system of configuration A with that associated with Fe states located as far as possible from the Co impurities. We see very clear resonances in the Co signal at −800 and +200 meV. The latter energy agrees quantitatively with the bias used to image Co atoms on the surface of lightly Co-doped Ca-122 in STM recently.[37] Note the present calculation also predicts that the Co should be visible as minima in the local tunnelling current relative to nearby Fe at −200 and +800 meV.

In addition to changes in the overall electronic structure of the system, we can consider the effective local potential due to Co, as would be used in a tight-binding Hamiltonian. For a discussion of this quantity and its calculation, see Ref. 38. To observe only the first-order effect, we calculated the total potential for a doped system where we did not allow relaxation, and subtracted the total potential for an undoped system. Figure 10 shows a number of line cuts of the potential change in the two-dimensional Fe plane, scaled to the average Fe-Fe distance $\langle a_{\text{Fe-Fe}}\rangle = 2.7972$ Å [note we use here the coordinate axes (x,y) aligned along the nearest-neighbor Fe-Fe bonds]. The directions are oriented according to the lines of collinear spins of the SDW state. The nonmagnetic potential variation is localized to roughly 1 Å from the dopant center, or about 0.25 of an average Fe-Fe distance. The oscillations visible in the figure occur near the core and originate from the difference in electron shell structure between Co and Fe, i.e., the larger Z for Co causes a difference in the radial shell structure as compared to Fe. In the spin

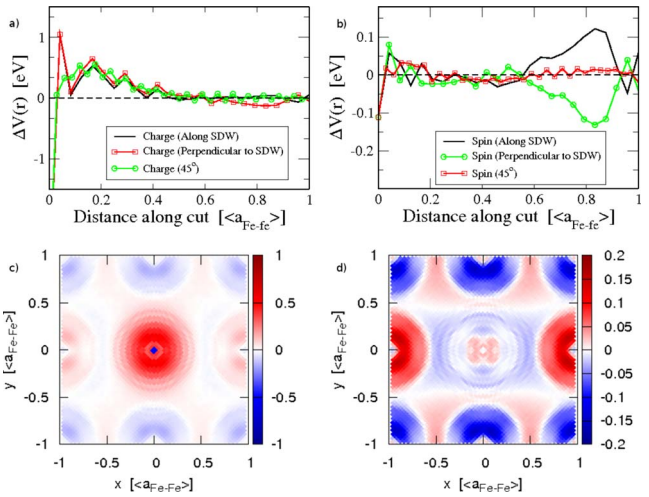

FIG. 10. (Color online) Top: line cuts of the potential change in the charge (left) and spin (right) channels upon Co doping. Bottom: cuts through the Fe plane of the same.

channel, the changes in potential occur mainly near the next iron site, indicating that there is a strong nonlocal effect in the magnetic behavior of the system. In *both* cases, it is clear that the collinear SDW state couples very strongly to the Co and drives a large anisotropy in the effective potential.

In models of correlated Fermi systems, a nonmagnetic impurity can induce magnetization on neighboring sites through its perturbation of the magnetic correlations in the host material; such effects are well known in quantum spin systems and high-T_c cuprates,[39] and can be qualitatively captured in mean field theories. The current calculation describes the intrinsic magnetic effects due to the Co ion itself, as well as induced magnetic effects of this type in the surrounding Fe system at the DFT level, and should be a good approximation to the actual potential due to the intermediate strength correlations in these systems. In the simplest cases, one expects such induced magnetic effects due to correlations to decay away from the impurity site with a length scale corresponding to the magnetic correlation length in the pure host. Here we note that, in contrast to the charge sector potential, we can detect no significant decay of the magnetic potential over the size of our unit cell at all, consistent with the long-range order present in the ground state. The long-range effect of this potential may be responsible for the rapid destruction of magnetic order by Co observed in this system.[14]

Calculations discussed thus far refer to the effect of a Co on the system in its SDW ground state. In principle, it is interesting to discuss the same questions in a host PM state. However, we find that the introduction of a Co in the PM state always induces a SDW state spanning our entire unit cell, in both the orthorhombic and tetragonal lattices, and for a number of initial conditions. This fact, coupled with the discussion above of the strong nonlocal component to the potential in the spin channel implies that in the PM state the scale on which the dopant affects the magnetic behavior is longer than our unit-cell size.

In a simple two-band phenomenological picture for the Fe plane used frequently in the literature, the two sheets of the Fermi surface are connected by a vector $(\pi/a,0)$ or $(0,\pi/a)$ in momentum space. Elastic electronic scattering processes which connect these sheets are referred to as interband, and are considered particularly important because they will break Cooper pairs in superconducting states like the currently popular "$s_{\pm}$" state proposed by Mazin *et al.* as a candidate for the ground state in the Fe-pnictide systems.[40] Since the spin potential shown in Fig. 10 is strongly peaked at a distance close to one Fe-Fe distance, a Fourier transform will be strongly peaked at precisely the interband scattering wave vectors. One might be tempted to deduce a strong interband scattering component for use in simple phenomenological models of Co as a localized elastic scatterer. This is incorrect, however, since the wave vectors must be considered in the magnetic Brillouin zone where the "interband" **q** are equivalent to zero in the system with long-range commensurate order.

We would nevertheless like to use the information from the DFT calculation to provide an input to phenomenological models, and therefore project the potential onto local atomic states, with the caveat that the following analysis is only valid in the system with long-range collinear magnetic order. To be able to map the potential to an on-site energy within a tight-binding model, the quantity needed is the matrix element of the potential in the appropriate Fe $3d$ orbital (which we denote by U_c^m),

$$U_c^m(\vec{R}) = \sum_{\sigma} \langle \phi_{l=2}^m(\vec{r}-\vec{R})|\Delta V_\sigma(\vec{r})|\phi_{l=2}^m(\vec{r}-\vec{R})\rangle, \qquad (1)$$

where we have used the radial atomic wave function from the pseudopotential. Table I lists projections of the matrix elements for various sites near the impurity. Note that there are two neighbors of each type, and we have reported the potential averaged on the two (although they do not deviate appreciably from the average).

In addition to scattering in the charge channel, it is also useful to calculate the scattering in the magnetic channel. To

TABLE I. Projections of the scattering potential onto d orbitals on both the cobalt dopant site and the nearest-neighbor Fe sites, in both the charge and spin channels. All values are in eV.

		Impurity site		Same-spin neighbor		Opposite-spin neighbor	
m	Orbitals	U_c^m	U_s^m	U_c^m	U_s^m	U_c^m	U_s^m
0	d_{z^2}	1.29	−0.331	0.572	0.709	−0.634	−0.639
±1	d_{xz}, d_{yz}	1.52	−0.378	0.672	0.848	−0.805	−0.733
±2	$d_{x^2-y^2}$, d_{xy}	1.87	−0.495	0.882	1.099	−0.956	−0.965

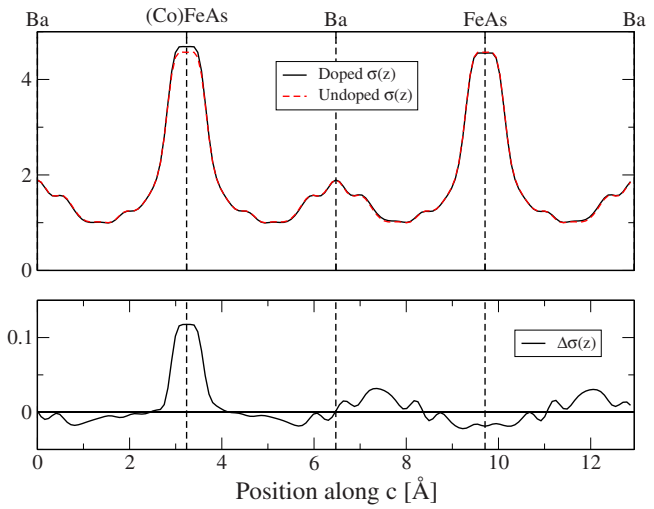

FIG. 11. (Color online) Top: linear integrated charge density for the doped and undoped systems, in number of electrons. Bottom: difference between doped and undoped linear integrated charge densities

do so, we calculate the difference between the spin-up and spin-down scattering potentials, projected onto the same iron $3d$ orbital

$$U_s^m(\vec{R}) = \sum_\sigma \langle \phi_{l=2}^m(\vec{r}-\vec{R}) | \sigma \Delta V_\sigma(\vec{r}) | \phi_{l=2}^m(\vec{r}-\vec{R}) \rangle, \qquad (2)$$

where σ is either $\frac{1}{2}$ or $-\frac{1}{2}$. The values found are shown in Table I. Note that the sign of the scattering in the spin channel will depend on which spin sublattice the Co dopant is located. As can be seen from the Table, as the cobalt ion changes the potential on the impurity site, it also induces significant nearest-neighbor potentials. The neighboring Fe sites with the same spin state repel both electrons and spin, and the sites in the perpendicular direction attract both.

We now consider the process by which Co dopes the FeAs plane. Figure 11 shows the linear integrated planar charge density $\sigma(z) = \int dxdyn(\vec{r})$ As can be seen from the figure, there is very little doping outside of a 2 Å range around the plane containing the Co dopant. There is, however, some shift of charge around the undoped plane, due to the relocation of the As atoms. However, integration around the planes finds that the net charge transferred to the undoped plane is zero, i.e., the whole doped electron remains in the dopant plane. We have verified that the doped electron is delocalized in this plane over the extent of our current unit cell (not shown).

The effective potential due to the dopant considered above will affect the surrounding density of states near the Co; in particular it may be interesting to consider the apparently long-range effect of the magnetic potential on states near the Fermi level. To this end we calculate the local density of states, integrated over a small range around the Fermi energy

$$\nu(\vec{r}) = \sum_\sigma \int_{E_F-\delta}^{E_F+\delta} d\omega \rho_\sigma(\vec{r},\omega), \qquad (3)$$

where we have chosen $\delta = 0.01$ eV. Figure 12(a) shows a cut of $\nu(\vec{r})$ through the undoped and doped Fe plane for configuration A. There is a clear modulation of the density of states in both planes; the modulation is commensurate with the spin-density wave, i.e., $\nu(\vec{r})$ is increased along the lines of majority spin, and suppressed along those of minority spin. Thus, the Co dopant in configuration A produces effects in the local DOS of the neighboring plane, even though it does not dope this plane. Figures 12(b) and 12(c) show cuts of $\nu(\vec{r})$ through one of the planes of configurations B and C. The atomic positions for configurations B and C are not optimized; we have, however, compared $\nu(\vec{r})$ for optimized and nonoptimized configuration A, and find that there is no appreciable qualitative difference. Since there are two Co dopants, depending on their location relative to the magnetic structure, there is the possibility of them being in the same- or opposite-spin states. Additionally, there will be interference effects based on their relative location, but we do not address this issue here. We have placed them as far apart as possible, and will restrict ourselves to considering the first-. effects on the local DOS. As can be seen from the figure, the clear stripes seen in the undoped plane of configuration A are not as pronounced in either configuration B or C. There is still some difference between the lines of up and down spins, but the contrast is markedly smaller. Since these effects occur in the total (spin-summed) local DOS, they may be visible in standard STM experiments. Even though the effect in configurations B and C is much smaller, the dopant distribution of the samples are not always uniform, as found in some NMR experiments.[18] So, all three configurations considered

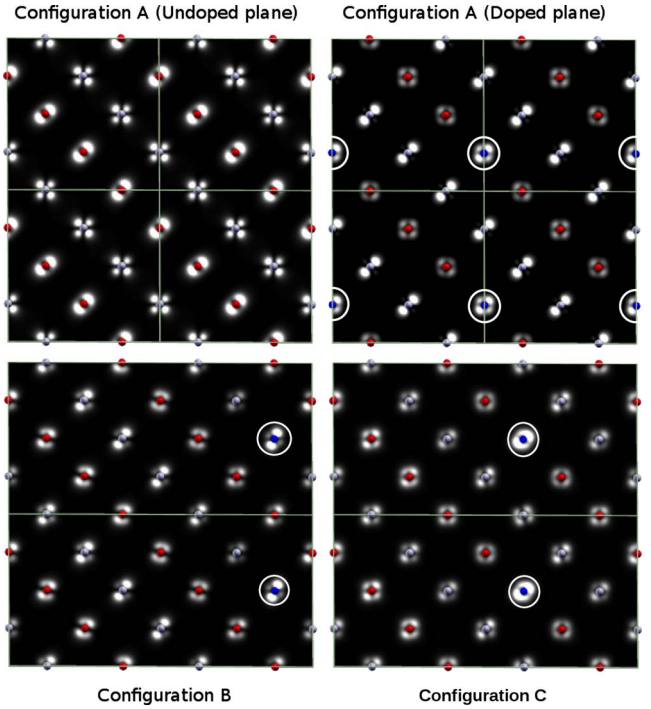

FIG. 12. (Color online) Plane cuts of the local Fermi level DOS [see Eq. (3)]. Red (gray) balls indicate Fe ion in the spin-down (-up) state. The Co dopant is indicated blue, has been circled where visible. Four unit cells are shown for configuration A, and two unit cells are shown for configurations B and C.

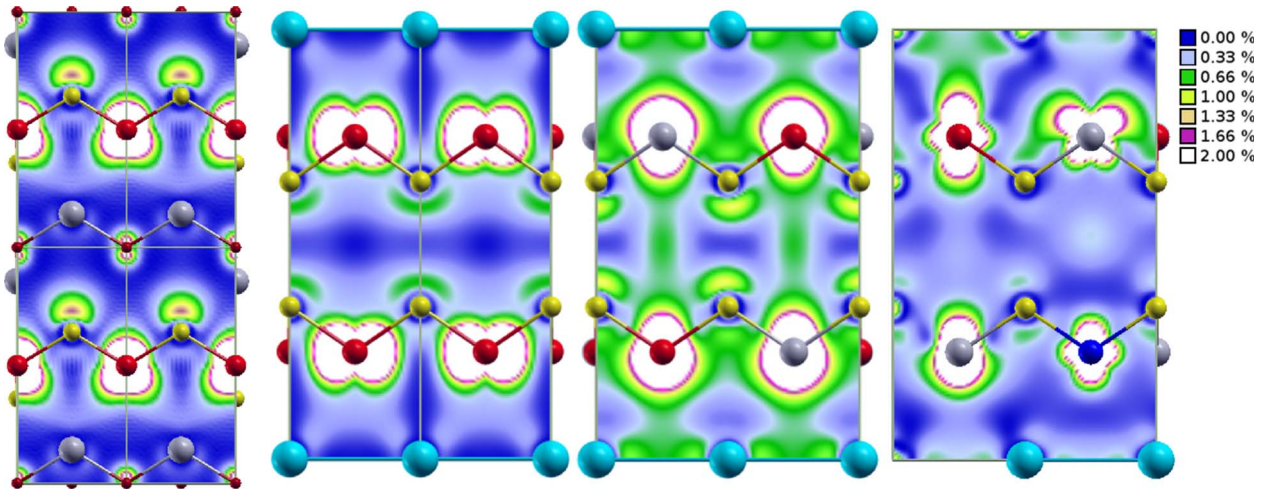

FIG. 13. (Color online) Cut of the local Fermi level DOS [see Eq. (3)] through the vertical plane FeAs plane for LaOFeAs in the PM state, $BaFe_2As_2$ in the PM state $BaFe_2As_2$ in the SDW state and $Ba(Fe_{1-x}Co_x)_2As_2$ ($x=\frac{1}{16}$) in configuration A. Colors are scaled from 0% to 2% of the maximum local DOS in the horizontal FeAs plane. For $BaFe_2As_2$ (undoped and in configuration A), red (gray) balls indicate spin-down (up) Fe atoms.

above are possibly visible experimentally. The importance of this result is to note that the long-range magnetic perturbation of a Co dopant on the spin system should have a significant effect modulating the electronic structure of the FeAs plane; depending on the nature of the Co-Co interference effects largely neglected here, these modulations may occur as well on longer length scales than our current unit-cell size, and may be responsible for the 8-Fe lattice spacing incoherent modulations reported in Ref. 37.

As mentioned above, critical field, transport and London penetration depth data appear to indicate that the 122 systems are considerably less two-dimensional than their 1111 counterparts.[24] In Fig. 13 we show the density of states integrated over a small range around the Fermi level ($\nu(\vec{r})$) along the plane perpendicular to (100). To illustrate the density of states present in between the FeAs layers, we have scaled the plots by the maximum found in the FeAs layer in each case. It is clear from the figure that $BaFe_2As_2$ has a larger Fermi level density of states available between the FeAs layers than LaOFeAs, which is not immediately visible from the band structure. This is true for both the PM and SDW states, suggesting that it is lattice structure rather than the magnetic state that is the cause for the difference. The distance between FeAs layers is roughly 3 Å less in $BaFe_2As_2$ than it is in LaOFeAs, accounting for the larger c-axis dispersion seen in the 122-structure materials[41] as compared to the 1111-type materials, whose Fermi surfaces are generally considered to be cylindrical. Furthermore, in LaOFeAs, the As z position is in phase from layer to layer, whereas in $BaFe_2As_2$ it is out of phase—the interlayer As atom pairs are alternately closer and farther (see Fig. 13). This explains the presence of additional states between the layers. Upon cobalt substitution, the density of states available in between the planes decreases (rightmost panel of Fig. 13), suggesting the Co doping increases the anisotropy. So far, the theoretical models for the pnictide superconductors have been limited to two dimensions. These results, as well as the experimental work,[19,23,24] suggest that a three-dimensional model is needed.

V. CONCLUSIONS

We have performed an in-depth study of cobalt doping and anisotropy in the oxygen-free pnictide superconductor $Ba(Fe_{1-x}Co_x)_2As_2$ for $x=\frac{1}{16}$. For this low doping, it is appropriate to consider the SDW state, which is quite different in nature from the PM state. Relative to the more commonly discussed PM electronic structure, in the SDW state the number of bands crossing the Fermi surface and the density of states at the Fermi level are reduced. Upon Co doping, the density of states at the Fermi level is shifted slightly, but there are other changes in local electronic structure which are not consistent with a rigid band shift. Co was found to only dope the plane where it resides, and the charge of one electron is spread over the entire plane as far as can be determined with our unit cell. Furthermore, it provides both a local and a nonlocal scattering potential, of roughly 1.5 eV in the charge channel, and 0.3 eV in the spin channel on the impurity site. The majority of the larger charge-channel potential is localized in a region of approximately 1 Å in size in real space. In addition, however, the Co breaks the spin degeneracy of the SDW state by introducing a net moment of $\sim 0.5\mu_B$/cell, and creates a significant and highly anisotropic nonlocal magnetic potential on the neighboring Fe orbitals whose range is larger than our current unit-cell size. This remarkable effect explains why Co is so effective in suppressing the SDW transition temperature.

We have furthermore investigated the effect of Co on the electronic states near the Fermi level. The Co states themselves are responsible for resonances we find at −800 and +200 meV, the latter of which has already been used by STM (Ref. 37) to image Co atoms on the surface of Co-doped Ca-122. A further intriguing consequence of the long-

range nature of the magnetic potential is that the Co induces a modulation of the local density of states aligned with the wave vector of the SDW state, which may also be visible by STM. The determination of the actual range of the magnetic influence of Co, and the effects of interference of many Co, which may lead to other longer range modulations of the system, will be pursued in a later study.

Finally, we have addressed the issue of the low anisotropy, comparing LaOFeAs and $BaFe_2As_2$ by examining the local density of states near the Fermi energy. We find there to be a larger number of states available between FeAs layers in both the PM and SDW state of $BaFe_2As_2$, partially due to the interlayer As position; this appears to be the cause for the lower anisotropy observed in experiment. Co doping appears to reduce the coupling between planes and therefore enhance the anisotropy. These results point to a need for three-dimensional models to properly describe these systems.

ACKNOWLEDGMENTS

This work was supported by DOE under Grants No. DE-FG02-02ER45995 (HPC) and No. DE-FG02-05ER46236 (PJH). We thank J. C. Davis, S. Pan, G. Sawatzky, and R. Valenti for helpful discussions, and H. Kontani for a useful suggestion. The authors acknowledge the University of Florida High-Performance Computing Center for providing computational resources and support that have contributed to the research results reported within this paper. URL: http://hpc.ufl.edu

*kemper@qtp.ufl.edu

[1] M. Rotter, M. Tegel, and D. Johrendt, Phys. Rev. Lett. **101**, 107006 (2008).
[2] N. Ni, S. L. Bud'ko, A. Kreyssig, S. Nandi, G. E. Rustan, A. I. Goldman, S. Gupta, J. D. Corbett, A. Kracher, and P. C. Canfield, Phys. Rev. B **78**, 014507 (2008).
[3] G. Wu, Y. L. Xie, H. Chen, M. Zhong, R. H. Liu, B. C. Shi, Q. J. Li, X. F. Wang, T. Wu, Y. J. Yan, J. Ying, and X. Chen, J. Phys.: Condens. Matter **21**, 142203 (2009).
[4] A. S. Sefat, R. Jin, M. A. McGuire, B. C. Sales, D. J. Singh, and D. Mandrus, Phys. Rev. Lett. **101**, 117004 (2008).
[5] S. Graser, T. A. Maier, P. J. Hirschfeld, and D. J. Scalapino, New J. Phys. **11**, 025016 (2009).
[6] K. Kuroki, S. Onari, R. Arita, H. Usui, Y. Tanaka, H. Kontani, and H. Aoki, Phys. Rev. Lett. **101**, 087004 (2008).
[7] X.-L. Qi, S. Raghu, C.-X. Liu, D. J. Scalapino, and S.-C. Zhang, arXiv:0804.4332 (unpublished).
[8] V. Barzykin and L. Gor'kov, JETP Lett. **88**, 131 (2008).
[9] Y. Bang and H.-Y. Choi, Phys. Rev. B **78**, 134523 (2008).
[10] Z.-J. Yao, J.-X. Li, and Z. Wang, New J. Phys. **11**, 025009 (2009).
[11] R. Sknepnek, G. Samolyuk, Y.-B. Lee, and J. Schmalian, Phys. Rev. B **79**, 054511 (2009).
[12] F. Wang, H. Zhai, Y. Ran, A. Vishwanath, and D.-H. Lee, Phys. Rev. Lett. **102**, 047005 (2009).
[13] A. V. Chubukov, D. V. Efremov, and I. Eremin, Phys. Rev. B **78**, 134512 (2008).
[14] P. C. Canfield, S. L. Bud'ko, N. Ni, J. Q. Yan, and A. Kracher, Phys. Rev. B **80**, 060501(R) (2009).
[15] S. Takeshita and R. Kadono, New J. Phys. **11**, 035006 (2009).
[16] X. F. Wang, T. Wu, G. Wu, R. H. Liu, H. Chen, Y. L. Xie, and X. H. Chen, New J. Phys. **11**, 045003 (2009).
[17] J. Chu, J. G. Analytis, C. Kucharczyk, and I. R. Fisher, Phys. Rev. B **79**, 014506 (2009).
[18] F. L. Ning, K. Ahilan, T. Imai, A. S. Sefat, R. Jin, M. A. McGuire, B. C. Sales, and D. Mandrus, J. Phys. Soc. Jpn. **78**, 013711 (2009).
[19] N. Ni, M. E. Tillman, J. Q. Yan, A. Kracher, S. T. Hannahs, S. L. Bud'ko, and P. C. Canfield, Phys. Rev. B **78**, 214515 (2008).
[20] R. T. Gordon, C. Martin, H. Kim, N. Ni, M. A. Tanatar, J. Schmalian, I. I. Mazin, S. L. Bud'ko, P. C. Canfield, and R. Prozorov, Phys. Rev. B **79**, 100506(R) (2009).
[21] Y. Laplace, J. Bobroff, F. Rullier-Albenque, D. Colson, and A. Forget, arXiv:0906.2125 (unpublished).
[22] C. Cao, P. J. Hirschfeld, and H.-P. Cheng, Phys. Rev. B **77**, 220506(R) (2008).
[23] M. A. Tanatar, N. Ni, C. Martin, R. T. Gordon, H. Kim, V. G. Kogan, G. D. Samolyuk, S. L. Bud'ko, P. C. Canfield, and R. Prozorov, Phys. Rev. B **79**, 094507 (2009).
[24] R. Prozorov, M. A. Tanatar, R. T. Gordon, C. Martin, H. Kim, V. G. Kogan, N. Ni, M. E. Tillman, S. L. Bud'ko, and P. C. Canfield, Physica C **469**, 582 (2009).
[25] W. Kohn and L. J. Sham, Phys. Rev. **140**, A1133 (1965).
[26] P. Hohenberg and W. Kohn, Phys. Rev. **136**, B864 (1964).
[27] S. Baroni, A. Dal Corso, S. de Gironcoli, P. Giannozzi, C. Cavazzoni, G. Ballabio, S. Scandolo, G. Chiarotti, P. Focher, A. Pasquarello, K. Laasonen, A. Trave, R. Car, N. Marzari, and A. Kokalj, http://www.pwscf.org
[28] J. P. Perdew, K. Burke, and M. Ernzerhof, Phys. Rev. Lett. **77**, 3865 (1996).
[29] M. Rotter, M. Tegel, D. Johrendt, I. Schellenberg, W. Hermes, and R. Pöttgen, Phys. Rev. B **78**, 020503(R) (2008).
[30] Q. Huang, Y. Qiu, W. Bao, M. A. Green, J. W. Lynn, Y. C. Gasparovic, T. Wu, G. Wu, and X. H. Chen, Phys. Rev. Lett. **101**, 257003 (2008).
[31] J. Zhao, W. Ratcliff II, J. W. Lynn, G. F. Chen, J. L. Luo, N. L. Wang, J. Hu, and P. Dai, Phys. Rev. B **78**, 140504 (2008).
[32] Y.-Z. Zhang, H. C. Kandpal, I. Opahle, H. O. Jeschke, and R. Valenti, arXiv:0812.2920 (unpublished).
[33] A. Leithe-Jasper, W. Schnelle, C. Geibel, and H. Rosner, Phys. Rev. Lett. **101**, 207004 (2008).
[34] A. S. Sefat, D. J. Singh, R. Jin, M. A. McGuire, B. C. Sales, and D. Mandrus, Phys. Rev. B **79**, 024512 (2009).
[35] D. Kasinathan, A. Ormeci, K. Koch, U. Burkhardt, W. Schnelle, A. Leithe-Jasper, and H. Rosner, New J. Phys. **11**, 025023 (2009).
[36] K. McElroy, H. Eisaki, S. Uchida, and S. C. Davis, Science **309**, 1048 (2005).
[37] T.-M. Chuang *et al.* (unpublished).
[38] L.-L. Wang, P. J. Hirschfeld, and H.-P. Cheng, Phys. Rev. B **72**, 224516 (2005).
[39] H. Alloul, J. Bobroff, M. Gabay, and P. J. Hirschfeld, Rev. Mod. Phys. **81**, 45 (2009).
[40] I. I. Mazin, D. J. Singh, M. D. Johannes, and M. H. Du, Phys. Rev. Lett. **101**, 057003 (2008).
[41] D. Singh, Phys. Rev. B **78**, 094511 (2008).